RESEARCH

Fatigue crack growth analysis of hydrogel by using peridynamics

Yujie Chen · Yang Yang · Yijun Liu

Abstract This study presents an application of bond-associated non-ordinary state-based peridynamics (PD) and the corresponding fatigue theory to predict fatigue crack growth in hydrogel. The constitutive model of the hydrogel is assumed to be the neo-Hookean material. Fatigue process is viewed as a series of quasi-static crack growth and solved by the explicit method. The applied strain energy-based fatigue criterion is obtained from hydrogel fatigue experiments. The fidelity of this model is established by simulating the relevant experiment. Due to the limitation of the test data, only crack growth phase of fatigue life of hydrogel is focused on. The progressive damage predictions by PD agree with that of experiment and capture the general characteristics of the experimentally observed damage patterns.

Keywords Bond-associated non-ordinary state-based peridynamics · Fatigue crack growth analysis · Hydrogel · Neo-Hookean

Y. Chen · Y. Yang (✉) · Y. Liu (✉)
Department of Mechanics and Aerospace Engineering, Southern University of Science and Technology, Shenzhen, China
e-mail: yangy33@sustech.edu.cn

Y. Liu
e-mail: liuyj3@sustech.edu.cn

1 Introduction

Over the past few decades, hydrogels have attracted ever-increasing interest from both academic and industrial fields (He and Lu 2010). The tunable properties and functions and facile preparation methods of the hydrogels lead to their various applications in biotechnology and engineering ranging from drug-delivery systems (Chang et al. 2010), cell-laden matrix (Yang et al. 2017), anti-fogging films (Xu et al. 2023), anti-fouling coatings (Zhang et al. 2021), to self-healing film (Zhu et al. 2022), soft robotics (Ying et al. 2021), and 3D printing technology (Takishima et al. 2021). Many of these applications require hydrogels to sustain cyclic stretch and release, and one of the major failure forms of hydrogel is fatigue fracture. Nevertheless, the fatigue life prediction of hydrogel is complex. The corresponding analysis is very few in the literature. There may be three likely reasons (Tang et al. 2017). First, synthetic hydrogels are a relatively new type of materials, and interest in their mechanical behavior started only after the commercialization of contact lenses in the 1960s and superabsorbent diapers in the 1980s. Second, fatigue fracture was not "mission-critical" in initial applications of hydrogels. Third, hydrogels in use may degraded or dehydrate before they rupture under cyclic load. However, with expanded applications of the hydrogel the life-limiting factors come out, and the study of fatigue fracture of hydrogels becomes an urgent issue. Such a study will aid the development of fatigue-resistant hydrogels,

and further, broaden the applications of hydrogels. This paper initiates a numerical study of fatigue fracture of hydrogels.

In terms of predicting crack growth, the traditional approaches based on continuum mechanics face conceptual and mathematical difficulties in terms of predicting crack nucleation and growth, especially for multiple crack paths, because the equations in classical continuum mechanics are derived by using spatial derivatives. Recently, peridynamics (PD) based on the non-local theory was developed by Dr. Silling (Silling 2000), which has aroused intense interest since it becomes a promising method to study crack propagation. It attempts to unify the mechanics of continuous and discontinuous media within the same framework in which the spatial derivatives are replaced by integrals, so that the PD governing equations are applicable to fractures and external crack growth criteria are no longer necessary. PD has been adopted to study brittle fracture (Yang and Liu 2022, 2021), failure in fiber-reinforced composites ((Zhou et al. 2017; Hu and Madenci 2016)), damage in functionally graded materials (Cheng et al. 2015, 2018), and crack path in polycrystal materials (Ghajari et al. 2014; Zhang et al. 2019).

PD also has been successfully applied to predict fatigue fracture. Silling and Askari (Silling and Askari 2014) introduced a PD model for fatigue cracking in metallic structures. It is based on the concept of remaining life and it is capable of predicting life concerning crack initiation and fatigue crack growth. Another PD fatigue model was proposed by Oterkus et al. (Oterkus et al. 2010) that applies only to the growth phase of a crack. Zhang et al. (Zhang et al. 2016) improved the computational efficiency of the model by Silling and Askari (Silling and Askari 2014), and investigated the fatigue cracking in metals and two-phase composites. Jung and Seok (Jung and Seok 2017) developed a mixed-mode fatigue crack growth analysis using PD approach to extend the fatigue model for mode I crack case. Hu and Madenci (Hu and Madenci 2017) presented an application of PD to predict damage initiation and growth in fiber reinforced composites under cyclic loading. A method for fatigue multi-crack propagation simulation based on ordinary state-based peridynamics was established by Zhao et al. (Zhao et al. 2019). Peridynamics with corrected boundary conditions was implemented by Ghaffari et al. (Ghaffari et al. 2019) in a hierarchical

multiscale method to study rolling contact fatigue. An energy-based PD model for fatigue cracking was proposed by Cong et al.(Cong et al. 2020). In their work, the definition of cyclic bond energy release rate range and the energy-based PD fatigue equations for both crack initiation and crack growth phases were introduced. A fatigue damage-cumulative model within PD framework was proposed to serve the needs of fatigue and damage tolerance evaluation in digital twin paradigm by Liu et al. (Liu et al. 2021). Based on the concept of fatigue element block and damage accumulation law in the form of Coffin-Manson relationship, the proposed model applied to both fatigue crack initiation and fatigue crack growth. Zhu et al. (Zhu et al. 2021) predicted the fatigue crack propagation in polycrystalline materials under cyclic loads using PD theory. However, due to the complex material constitutive model and large deformation characteristic, there exists no PD model to predict fatigue damage in hydrogel. The conventional strain energy-based criterion for fatigue simulation is based on the theoretical strain field at the crack tip of a linear elastic solid (Cong et al. 2020). Nevertheless, such derivation is not suitable for hyperelastic material, since the strain and stress state at the crack tip is different from linear elastic material and the theoretical strain field at the crack tip can be hardly derived. Therefore, a different approach should be performed to obtain the strain energy-based criterion.

In this work, the neo-Hookean model is taken as the material constitutive model to describe the stress-stretch response of hydrogel under a large tensile stretch. Based on the bond-associated non-ordinary state-based peridynamic and the fatigue theory, the fatigue crack growth analysis of hydrogel is presented. The fatigue loading is simulated by considering incremental static analyses of cyclic loads with constant amplitude. Dynamic PD equilibrium equation is solved by employing explicit techniques, adding a damping term to stabilize the computation. Fatigue propagation of the hydrogel crack is predicted by employing strain energy density-based criteria according to the experiments. The simulation yields the number of cycles till the propagation of damage, and the number of cycles for the extent of damage propagation. The fatigue prediction of the hydrogel is validated by simulating the physical tests conducted by the work of Tang et al. (Tang et al. 2017).

The outline of this paper is as follows. After the introduction, the detailed experimental results of fatigue test on the polyacrylamide hydrogel are presented in Sec. 2. Theory of non-ordinary based peridynamics and neo-Hookean model is briefly described in Sec. 3. The fatigue failure theory in the framework of PD is introduced in Sec. 4. The implementation of fatigue crack growth in two-dimensional hydrogel sheet under pure shear modeling and simulation is discussed in Sec. 5, followed by the conclusions in Sec. 6.

2 Experimental observation

Tang et al. (Tang et al. 2017), conducted the fatigue test on the typical hydrogel samples: polyacrylamide hydrogel, which is readily synthesized in laboratories, and is used in many applications (Tang et al. 2017). The pre-notched samples were loaded cyclically in the pure shear test. As illustrated in Fig. 1a. The hydrogel sample can be roughly divided into three parts as shown in Fig. 1b. Zone I can be regarded as pristine and totally elastic. Zone II is under fatigue fracture containing process zone and stress concentration around the crack tip. Zone III is slack without elastic strain energy. The process of crack propagation is just the shrink of Zone I as Zone II moving leftward. The state of the crack tip remained the same.

Here we denote the stretch of Zone I along the loading direction as λ_{bulk}. The horizontal shrink of Zone I can be neglected. Then, owing to incompressibility, the stretch along the thickness direction is $1/\lambda_{bulk}$. Drawing in a Mohr's circle, this deformation state can be achieved by shear stress solely. Thus, this kind of experiment is called pure shear test, which has been widely performed on rubber-like materials (Rivlin and Thomas 1997, David et al. 2019).

The pure shear test of an intact sample (conducted in Ref. (Tang et al. 2017)) states that the constitutive relation of hydrogel can be described by the neo-Hookean model as

$$W = \frac{\mu}{2}(\lambda_1^2 + \lambda_2^2 + \lambda_3^2 - 3) \tag{1}$$

where λ_1, λ_2 and λ_3 are the principal stretches. In the pure shear test, replacing λ_1, λ_2 and λ_3 by λ_{bulk}, 1 and

Fig. 1 Illustration of the pure shear test. **a** Initial state. **b** Deformed state

(a)

(b)
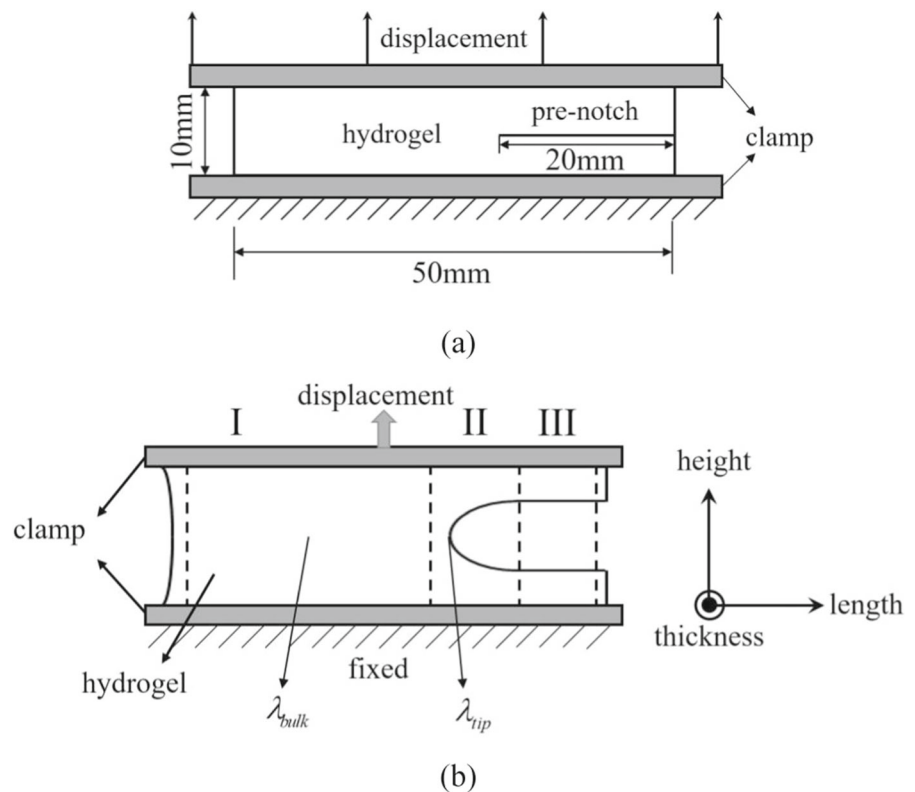
$1/\lambda_{bulk}$ respectively, the strain energy density for pure shear test or for Zone I can be written as

$$W(\lambda_{bulk}) = \frac{\mu}{2}(\lambda_{bulk}^2 + \lambda_{bulk}^{-2} - 2) \qquad (2)$$

The energy release rate G can be expressed as

$$G = HW(\lambda_{bulk}) \qquad (3)$$

where H is the initial height of the sample sheet. Experiments in Ref. (Tang et al. 2017) showed there is a linear relation between energy release rate and crack propagation speed, which can be fitted as

$$\frac{da}{dN} = 1.99 \times 10^{-8} \times (G - 7.03) \qquad (4)$$

where a is the crack length with unit of millimeter, N is the number of loading cycle. The intercept 7.03 J/m^2 is the fatigue threshold described in energy release rate G. If G is under this threshold, fatigue fracture will not occur. Detailed preparation process of this hydrogel samples is described in Ref. (Tang et al. 2017).

3 Peridynamic model of hydrogel

3.1 PD correspondence model for neo-Hookean material

Assume an object occupies a certain spatial domain in the reference configuration at time t. Based on non-local interactions, a material point represented by its initial position vector $\mathbf{x}$ interacts with other material points $\mathbf{x}'$ which are within a certain domain (horizon) denoted by $H_{\mathbf{x}}$. Conventionally, $H_{\mathbf{x}}$ is a circular (2D) or spherical (3D) region with a radius of δ. The bond vector is de fined as $\xi = \mathbf{x}' - \mathbf{x}$. According to Newton's second law, the PD equation of motion for a unit volume centered at material point $\mathbf{x}$ is written as

$$\rho(x)\ddot{\mathbf{u}}(x,t) = \int_{H_x} (\mathbf{t} - \mathbf{t}')dV_{x'} + \mathbf{b}(x,t) - c\dot{\mathbf{u}}(\mathbf{x},t) \qquad (5)$$

The integro-differential equation given in Eq. (5) can also be represented in a discrete form as

$$\rho_k\dot{\mathbf{u}} = \sum_{j=1}^{M_k} (\mathbf{t}_{kj} - \mathbf{t})V_j + \mathbf{b}_k - C\dot{\mathbf{u}}_k \qquad (6)$$

where ρ is the mass density, u, $\dot{\text{u}}$ and $\ddot{\text{u}}$ are the displacement, velocity and acceleration vectors, respectively; b is the body force density vector; $\mathbf{t}$ and $\mathbf{t}'$ are the pair-wise force density vectors, representing the interaction between the material points; c is a positive number denoting the numerical damping term. The subscripts represent the index of material point. In the following sections, this kinetic equation is used to find the quasi-static solution of the numerical model with an appropriate c. In this analysis, based on the experience, c is taken as shear modulus multiplying by 0.18.

In Eq. (6), M_k represents the number of family members of the material point k and j represents the family member of the material point k. The term V_j is the volume of the material point j. The term $\mathbf{t}_{kj}$ denotes the force density that the material point j exerts on the material point k, and $\mathbf{t}_{jk}$ corresponds to the force density that material point k exerts on the material point j.

Non-ordinary state-based PD gives the PD expression of deformation gradient, making it convenient to connect with traditional constitutive model. Bond-associated scheme is proposed to overcome the numerical instability and oscillation in non-ordinary state-based PD ((Behera et al. 2020; Roy et al. 2020)). As is shown in Fig. 2, for a bond vector ξ from x to $\mathbf{x}'$, its bond-associated deformation gradient tensor is computed by considering the intersection region of $H_{\mathbf{x}}$ and $H_{\mathbf{x}'}$.

In bond-associated scheme, the deformation gradient tensor is written as

$$\mathbf{F}_\xi(\mathbf{x}) = \left\{ \int_{H_{\mathbf{x}} \cap H_{\mathbf{x}'}} w[(\mathbf{y}'' - \mathbf{y}) \otimes (\mathbf{x}'' - \mathbf{x})]dV_{\mathbf{x}''} \right\} \mathbf{K}_\xi^{-1} \qquad (7)$$

where $\mathbf{x}''$ and $\mathbf{y}''$ are the position vectors in reference and deformed configuration, respectively. $\mathbf{K}$ is the shape tensor expressed as

$$\mathbf{K}_\xi(\mathbf{x}) = \int_{H_{\mathbf{x}} \cap H_{\mathbf{x}'}} w[(\mathbf{x}'' - \mathbf{x}) \otimes (\mathbf{x}'' - \mathbf{x})] dV_{\mathbf{x}''} \qquad (8)$$

where w is the weight function evaluating the proportion of each point in the horizon.

The force density is associated with the first Piola–Kirchhoff stress tensor $\mathbf{P}$ as:
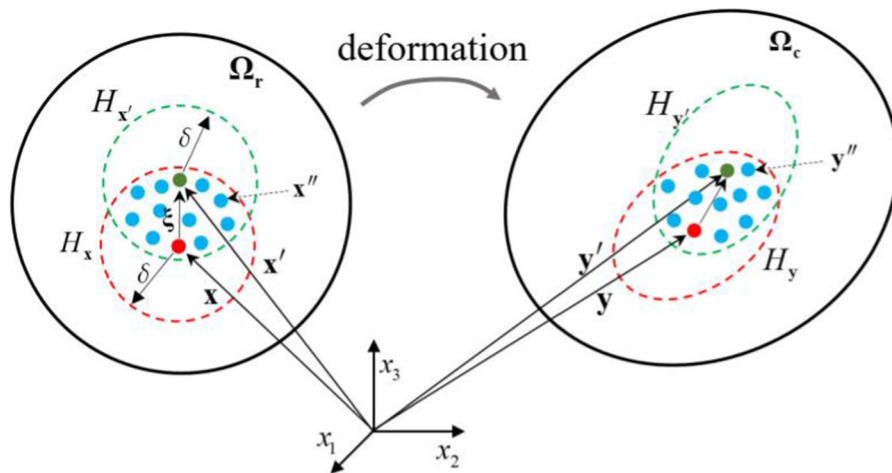
Fig. 2 Bond-associated scheme diagram

$$\mathbf{t}_\xi(\mathbf{x}) = \frac{1}{2} \frac{\phi_\xi(\mathbf{x}, \mathbf{x}')}{\phi(\mathbf{x}, \mathbf{x}')} w \mathbf{P}_\xi \mathbf{K}_\xi^{-1}(\mathbf{x}' - \mathbf{x}) \qquad (9)$$

with

$$\phi_\xi(\mathbf{x}, \mathbf{x}') = \frac{\int_{H_\mathbf{x} \cap H_{\mathbf{x}'}} dV_{\mathbf{x}''}}{\int_{H_\mathbf{x}} dV_{\mathbf{x}''}}$$

$$\phi(\mathbf{x}, \mathbf{x}') = \frac{\int_{H_{\mathbf{x}'}} dV_{\mathbf{x}''}}{\int_{H_{\mathbf{x}'}} dV_{\mathbf{x}''} + \int_{H_\mathbf{x}} dV_{\mathbf{x}''}} \qquad (10)$$

The selection of an appropriate material constitutive model is a tradeoff between accuracy and complexity. Behera et al. (Behera et al. 2020) derived the expression of the first Piola–Kirchhoff stress tensor of neo-Hookean material with slight compressibility, where the strain energy density function is expressed as

$$W = \frac{\mu}{2}(\bar{I}_1 - 3) + \frac{K}{8}(J - \frac{1}{J})^2 \qquad (11)$$

in which μ and K are shear and bulk moduli respectively; J is the determinant of $\mathbf{F}$, that is $J = \det \mathbf{F}$; $\bar{I}_1 = J^{-2/3} tr\mathbf{C}$ is the normalized first invariant with $\mathbf{C} = \mathbf{F}^T \mathbf{F}$. In the following sections, plane stress case is assumed. The corresponding expression of $\mathbf{P}$ is written as

$$\mathbf{P} = \mu(\mathbf{F} - C_{33}\mathbf{F}^{-T})C_{33}^{1/3}J^{-2/3} \qquad (12)$$

where C_{33} is the component of $\mathbf{C}$ which can be obtained numerically from the equation:

$$\mu(\frac{2}{3}C_{33}^{-2/3} - \frac{1}{3}C_{33}^{-1/3}tr\mathbf{C})J^{-2/3} + \frac{K}{4}(C_{33}J^2 - C_{33}^{-1}J^{-2}) = 0 \qquad (13)$$

Note that the deformation gradient tensor $\mathbf{F}$ in Eqs. (12) and (13) is 2 by 2 for 2D case. After computing the force density of the material points, the dynamic equation can be solved by using the explicit method, the acceleration, velocity, and displacement for each material points can be obtained at each step.

4 Peridynamics for fatigue crack based on cyclic bond strain energy density

In PD, description of failure is described by removing the interactions between points, i.e., bond breakage. In fatigue modeling (Silling and Askari 2014), a variable named "remaining life" φ_{kj}^N, is introduced to a bond connecting $\mathbf{x}_k$ to any point $\mathbf{x}_j$ in its horizon. The remaining life gradually reduces as the loading cycle N^{th} increases. For fatigue crack grow phase (phase II), the remaining life is usually represented by the bond strain (Silling and Askari 2014), which is replaced by the relationship between remaining life and the bond strain energy density in this analysis, as is performed in Ref. (Cong et al. 2020). By considering the fatigue threshold, the bond remaining life relates to bond strain energy density as

$$\varphi_{kj}^{N=0} = 1, \frac{d\varphi_{kj}^{N}}{dN} = \begin{cases} -A(\varepsilon_{kj}^{N} - \varepsilon_{\infty})^{B}, & \text{if } \varepsilon_{kj}^{N} > \varepsilon_{\infty} \\ 0 & \text{otherwise} \end{cases}. \tag{14}$$

where ε_{kj}^{N} is the strain energy density of the bond at N^{th} loading, ε_{∞} is the fatigue limit which is the lowest cyclic bond strain energy density that still results in fatigue damages. Material parameter A is a positive parameter and B is a positive constant exponent, which are to be calibrated from experiments. In contrast, A cannot be obtained directly from the fatigue equations obtained in experiments. However, A can be obtained by performing a simulation once with an arbitrary A_{trail} value (Cong et al. 2020) and the fatigue equation of experiments as:

$$A = A_{trail} \frac{(da/dN)_{(\text{exp}eriment)}}{(da/dN)_{(trail)}} \tag{15}$$

The negative bond remaining life means the bond broke irreversibly due to fatigue damage. In order to record the breakage of each bond, a history-dependent function γ is introduced:

$$\gamma_{kj}^{N} = \begin{cases} 1, & \text{if unbroken for all } 0 \leq N' \leq N \\ 0, & \text{if broken} \end{cases}. \tag{16}$$

The damage at material point j can be calculated as

$$D_{k}^{N} = 1 - \frac{\sum_{j=1}^{M_{k}} \gamma_{kj}^{N} V_{j}}{\sum_{j=1}^{M_{k}} V_{j}} \tag{17}$$

As is stated in Ref. (Cong et al. 2020), fatigue crack growth phase, i.e., phase II is valid for a bond of material point j when point j or at least one of its family members have $D \geq D_{0}$. Otherwise, it is under phase I. Here D_{0} is set 0.39 since the damage at a mode I crack tip is around 0.39 when $\delta = 3.015dx$.

In this article, we focus on phase II fatigue only, since experiments on the initiation of fatigue crack of hydrogel without a pre-cut is very limited.

5 Numerical implementation

In this section, a rectangular hydrogel sheet with a pre-notch of 20 mm is studied. The width and length of the sheet are 10 mm and 50 mm, respectively, as shown in Fig. 3. As is calibrated in Ref. (Tang et al. 2017), the
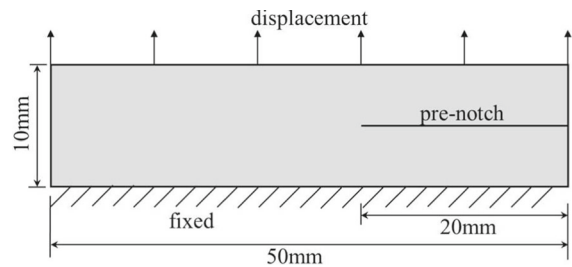
Fig. 3 Illustration of the sample geometry
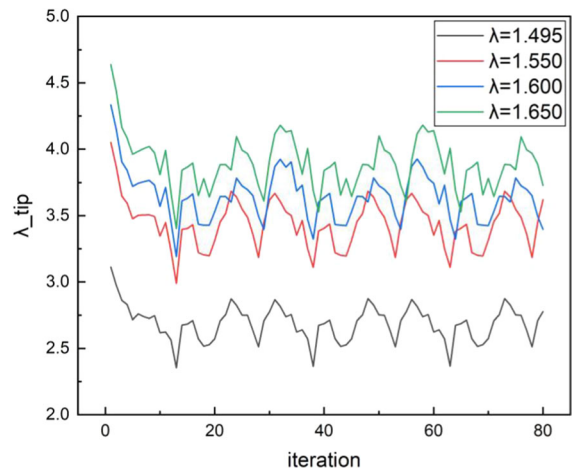
Fig. 4 Stretch at crack tip at each iteration step

shear modulus of the sample is 3.06 kPa. This value is applied in the following numerical samples.

5.1 Relation between λ_{bulk} and λ_{tip} in PD modeling

In PD modeling, 150×30 points are distributed uniformly to represent the hydrogel sheet. Thus, the spatial discretization size dx is 1/3 mm. The bonds crossing through the notch are broken to represent the initial crack. The top edge of the sheet is subjected the displacement loading until λ_{bulk} reaches the target value. In this analysis, the simulations were performed at $\lambda_{bulk} = 1.495$, 1.55, 1.60 and 1.65 which are same with the experiment. Note that when λ_{bulk} is 1.495, the energy release rate G is at its critical value 7.03 J/m^2, which is obtained according to Eq. (3). Then an iteration was performed: two or three bonds with the largest stretches were broken at each iteration step and their crack tip stretches are recorded. The stretch of a bond is defined as the current length of the bond divided by the initial length. Quasi-static solution was

Table 1 Quantities associated with different loading stretches

λ_{bulk}	λ_{tip}	$\varepsilon_{bulk}(\mathrm{kJm}^{-3})$	$\varepsilon_{tip}(\mathrm{kJm}^{-3})$	$\varepsilon_{tip} - \varepsilon_{\infty}(\mathrm{kJm}^{-3})$	$da/dN(10^{-4}\ \mathrm{mm/N})$
1.495	2.68	0.70	7.54	0	0
1.550	3.42	1.25	14.20	6.66	10.92
1.600	3.63	1.45	16.41	8.72	14.94
1.650	3.88	1.67	19.21	11.69	19.18

Fig. 5 Linear relation between dc/dN and $\varepsilon_{tip} - \varepsilon_{\infty}$
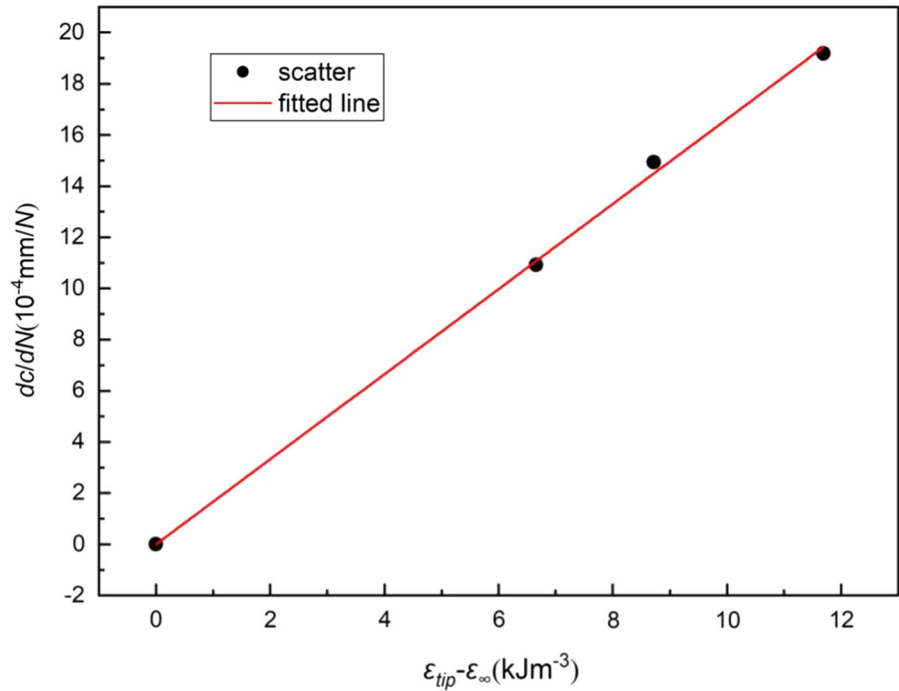
achieved after the breakage in each iteration step. The crack propagated for a small distance in each step and the average recorded crack tip stretches are plot in Fig. 4 with respect to iteration steps.

It can be observed that the stretch at the crack tip experienced a significant plunge during the first twelve iterations and then showed a periodic fluctuation. This periodic fluctuation is due to the periodic discretization of material points. We calculated the average value in a period as the stretch at the crack tip as crack propagating. The average crack tip stretches are 2.68, 3.42, 3.63 and 3.88 respectively, as listed in Table 1.

5.2 Relation between ε_{tip} and $\frac{da}{dN}$

The Mode I crack tip of the hyperelastic material can be regarded as an arc shape (Majid and Ayatollahi 2016). We use the crack tip stretch calculated in the previous part as the principal stretch of the material at the crack tip and the principal stretches can be approximated as $\lambda_1, \lambda_2, \lambda_3 = \lambda_{tip}, \lambda_{tip}^{-1/2}, \lambda_{tip}^{-1/2}$ respectively. Thus, the strain energy density at the crack tip associated with a bond can be written as $\varepsilon(\lambda_{tip}) = \frac{\mu}{2}(\lambda_{tip}^2 + 2/\lambda_{tip} - 3)$. The crack propagation speed $\frac{da}{dN}$ can be calculated by Eq. (4) according to loading stretch. The calculated data is shown in Table 1.

There is a linear relation between $\varepsilon_{tip} - \varepsilon_{\infty}$ and dc/dN, as shown in Fig. 5. Thus, parameter B in Eq. (14) is set to 1.

5.3 Fatigue simulation

To start with a quasi-static computation, the bond stretches at $\lambda = \lambda_{bulk}$ are obtained. Then an iteration for fatigue simulation is conducted. In each iteration

Fig. 6 Flow chart of the fatigue crack growth of hydrogel
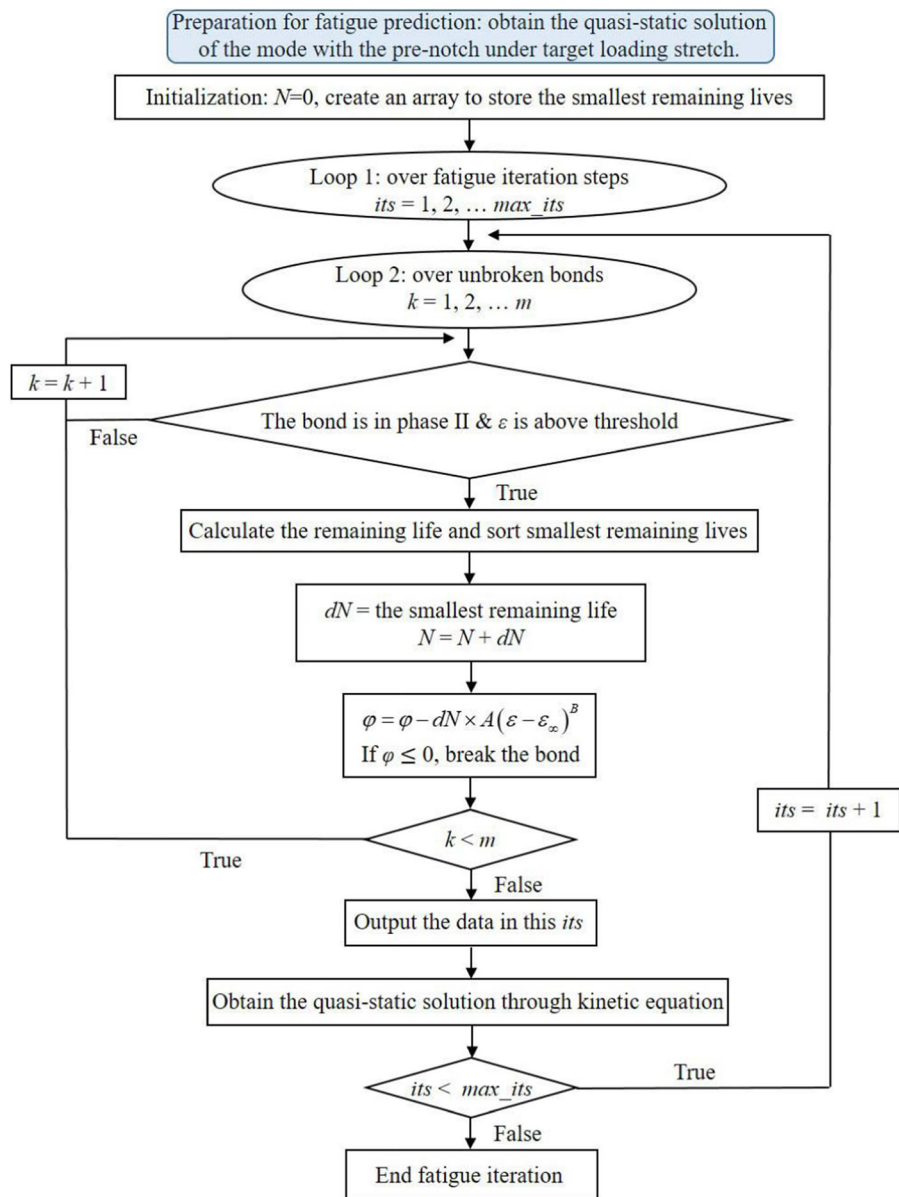
step, for the bonds undergoing phase II fatigue damage, their remaining cycles are calculated as

$$N_{remain(jk)} = \frac{\varphi_{kj}^N}{A(\varepsilon_{kj}^N - \varepsilon_\infty)} \qquad (18)$$

The remaining cycles of bonds are sorted from smallest to largest in an array as $\{N_{remain}^1 \quad N_{remain}^2 \quad ... \quad N_{remain}^n\}$. Considering efficiency, we break two or three bonds with the smallest lives at one iteration step rather than a single one. Besides, if too many bonds are broken at one step, the

accuracy can be lower and the valid points in the intersection region of H_x and $H_{x'}$ may be not enough, leading to the singularity of the shape tensor $\mathbf{K}_\xi$ in Eq. (7). There exist some extra methods to deal with such singularity, but actually the singularity may be avoided by just breaking two or three bonds at one step. Then each bond life is updated according to Eq. (14) undergoing N_{remain}^2 or N_{remain}^3 cycles. Note that in programming, loading cycle N can be treated as a real number instead of an integer. After the breakage in each step, a quasi-static solution is achieved. The

(a)

(b)

(c)

(d)
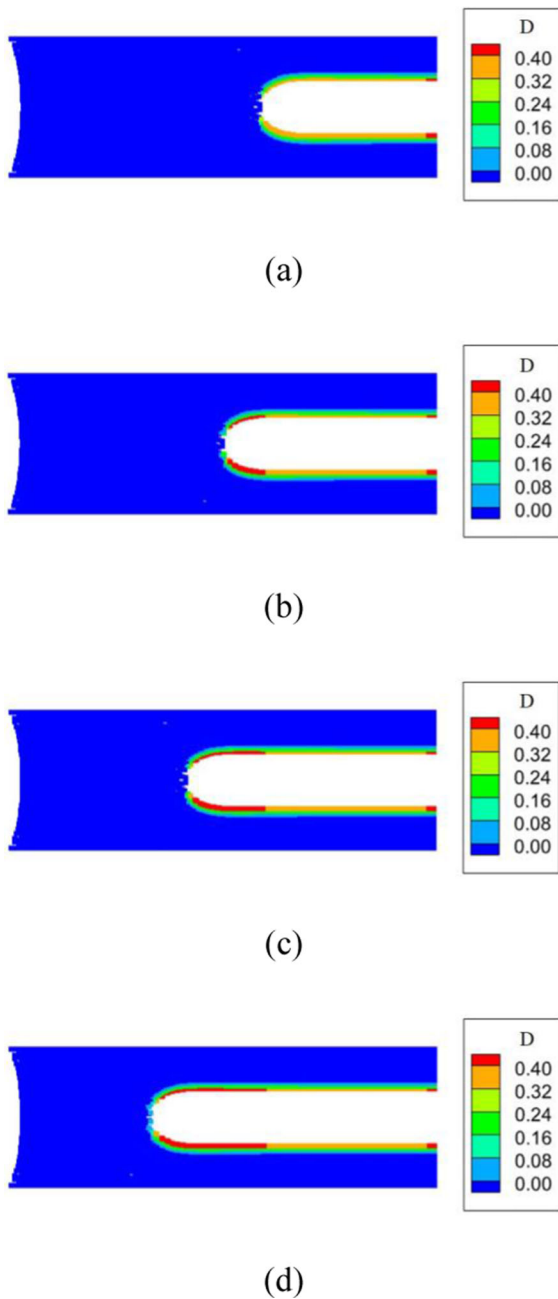
Fig. 7 a $da = 0$ mm, $N = 0$; **b** $da = 5$ mm, $N = 2564$; **c** $da = 10$ mm, $N = 5211$; **d** $da = 15$ mm, $N = 7782$

flow chart of the fatigue crack growth procedure is presented in Fig. 6.

Some steps of damage contour are presented in Fig. 7 under $\lambda_{bulk} = 1.65$. The average stretch at the crack tip in fatigue prediction is in coincidence with the recorded stretches in Sect. 5.1. After calibrating
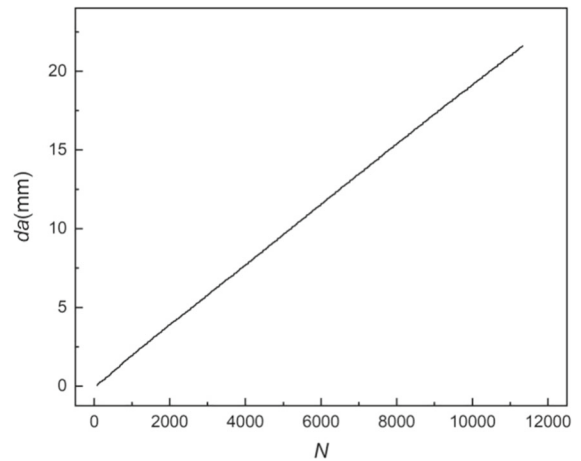
Fig. 8 Crack propagation length with respect to loading cycles

from the experiments, parameter A in Eq. (14) is set to 1.74×10^{-3}. The crack propagation length is 0 mm, 5 mm, 10 mm and 15 mm in Fig. 7a–d and the corresponding loading cycles are 0, 2564, 5211 and 7782 respectively. Figure 8 shows the crack propagation length da with respect to loading cycles N, which is in good agreement with prediction from Eq. (4) setting $\lambda_{bulk} = 1.65$.

Moreover, the fatigue model based on strain energy density is not limited in simulating pure shear test or Mode I crack, since such criterion has been applied in many other loading conditions on rubber-like materials (Mars and Fatemi 2002).

6 Conclusions

The fatigue crack growth of a hydrogel sheet under cyclic loading is analyzed by a bond-associated non-ordinary state-based peridynamics and the corresponding fatigue theory. The neo-Hookean model is employed as the material constitutive model in the dynamic equation and an appropriate damping term is adopted to keep the results stable. The fatigue implementation utilizes the fatigue data of the pure shear experiments. Present predicted crack propagation length with respect to loading cycles is in good agreement with experimental observation.

Declarations

Competing interests The authors declare no competing interests.

References

Behera D, Roy P, Madenci E (2020) Peridynamic correspondence model for finite elastic deformation and rupture in Neo-Hookean materials. Int J Non-Linear Mech 126:103564

Chang C, Duan B, Cai J, Zhang L (2010) Superabsorbent hydrogels based on cellulose for smart swelling and controllable delivery. Eur Polymer J 46(1):92–100

Cheng Z, Zhang G, Wang Y et al (2015) A peridynamic model for dynamic fracture in functionally graded materials. Compos Struct 133:529–546

Cheng Z, Liu Y, Zhao J et al (2018) Numerical simulation of crack propagation and branching in functionally graded materials using peridynamic modeling. Eng Fract Mech 191:13–32

Cong TN, Oterkus S, Oterkus E (2020) An energy-based peridynamic model for fatigue cracking. Eng Fract Mech 241(4):107373

David R, Julie D, Mathias et al (2019) Critical strain energy release rate for rubbers: single edge notch tension versus pure shear tests. Int J Fract 216:31–39

Ghaffari MA, Gong Y, Attarian S et al (2019) Peridynamics with corrected boundary conditions and its implementation in multiscale modeling of rolling contact fatigue. J Multiscale Model 10:1

Ghajari M, Iannucci L, Curtis P (2014) A peridynamic material model for the analysis of dynamic crack propagation in orthotropic media. Comput Method Appl Mech Eng 276(7):431–452

He X, Lu Q (2010) Design and fabrication strategies of cellulose nanocrystal-based hydrogel and its highlighted application using 3D printing: a review. Carbohydr Polym 301:120351

Hu YL, Madenci E (2016) Bond-based peridynamic modeling of composite laminates with arbitrary fiber orientation and stacking sequence. Compos Struct 153:139–175

Hu YL, Madenci E (2017) Peridynamics for fatigue life and residual strength prediction of composite laminates. Compos Struct 160:169–184

Jung JY, Seok J (2017) Mixed-mode fatigue crack growth analysis using peridynamic approach. Int J Fatigue 103:591–603

Liu B, Bao R, Sui F (2021) A fatigue damage-cumulative model in peridynamics. Chin J Aeronaut 34(2):329–342

Majid R, Ayatollahi M et al (2016) A new criterion for rupture assessment of rubber-like materials under mode-i crack loading: the effective stretch criterion. Adv Eng Mater 18(8):1364–1370

Mars WV, Fatemi A (2002) A literature survey on fatigue analysis approaches for rubber. Int J Fatigue 24:949–961

Oterkus E, Guven I, Madenci E (2010) Fatigue failure model with peridynamic theory. IEEE Intersociety Conference on Thermal and Thermomechanical Phenomena in Electronic Systems, Las Vegas, NV

Rivlin RS, Thomas AG (1997) Rupture of rubber. I. characteristic energy for tearing. J Polym Sci 3:291–318

Roy P, Behera D, Madenci E (2020) Peridynamic simulation of finite elastic deformation and rupture in polymers. Eng Fract Mech 236:107226

Silling SA (2000) Reformulation of elasticity theory for discontinuities and long-range forces. J Mech Phys Solids 48(1):175–209

Silling SA, Askari A (2014) Peridynamic model for fatigue cracking. Sandia Report 18590

Takishima Y, Yoshida K, Khosla A, Kawakami M, Furukawa H (2021) Fully 3D-printed hydrogel actuator for jellyfish soft robots. ECS J Solid State Sci Technol 10(3):037002

Tang JD, Li J, Vlassaka JJ, Suo ZG (2017) Fatigue fracture of hydrogels. Extreme Mech Lett 10:24–31

Xu X, Zhu T, Zheng W, Xian C, Huang J, Chen Z, Lai Y (2023) A robust and transparent hydrogel coating for sustainable antifogging with excellent self-cleaning and self-healing ability. Chem Eng J 451:137879

Yang Y, Liu YJ (2021) Modeling of cracks in two-dimensional elastic bodies by coupling the boundary element method with peridynamics. Int J Solids Struct 217–218:74–89

Yang Y, Liu YJ (2022) Analysis of dynamic crack propagation in two-dimensional elastic bodies by coupling the boundary element method and the bond-based peridynamics. Comput Methods Appl Mech Eng 399:115339

Yang X, Liu G, Peng L, Guo J, Tao L, Yuan J, Zhang L (2017) Highly efficient self-healable and dual responsive cellulose-based hydrogels for controlled release and 3D cell culture. Adv Func Mater 27(40):1703174

Ying B, Chen RZ, Zuo R, Li J, Liu X (2021) An anti-freezing, ambient-stable and highly stretchable ionic skin with strong surface adhesion for wearable sensing and soft robotics. Adv Func Mater 31(42):2104665

Zhang G, Le Q, Loghin A, Subramaniyan A, Bobaru F (2016) Validation of a peridynamic model for fatigue cracking. Eng Fract Mech 162:76–94

Zhang H, Li H, Ye H et al (2019) A coupling peridynamic approach for the consolidation and dynamic analysis of saturated porous media. Comput Mech 64(4):1097–1113

Zhang Z, Wang S, Liu G, Hu D, Yang B, Dai Q, Dou Q (2021) Antifouling hydrogel film based on a sandwich array for salivary glucose monitoring. RSC Adv 11(44):27561–27569

Zhao S, Yin Y, Wu X (2019) Ordinary state-based peridynamics method for fatigue multi-crack propagation. J Harbin Inst Technol 51(4):19–25

Zhou W, Liu D, Liu N (2017) Analyzing dynamic fracture process in fiber-reinforced composite materials with a peridynamic model. Eng Fract Mech 178:60–78

Zhu N, Kochan C, Oterkus E et al (2021) Fatigue analysis of polycrystalline materials using Peridynamic Theory with a novel crack tip detection algorithm. Ocean Eng 222:108572

Zhu M, Ying D, Zhang H, Xu X, Chang C (2022) Self-healable hydrophobic films fabricated by incorporating natural wax into cellulose matrix. Chem Eng J 446:136791